International Journal of Pharmaceutics 637 (2023) 122882

Contents lists available at ScienceDirect

International Journal of Pharmaceutics

journal homepage: www.elsevier.com/locate/ijpharm

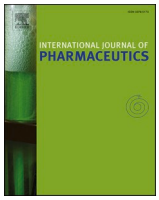

Rheological and low field NMR characterization of hydrophobically-modified PEG hydrogels for drug delivery

Michela Abrami [a], Fabio Bignotti [b], Francesco Baldi [b], Gloria Spagnoli [b], Alice Biasin [a], Lucia Grassi [a], Gabriele Grassi [c], Mario Grassi [a,*]

[a] Department of Engineering and Architecture, University of Trieste, Via Valerio 6/A, I-34127 Trieste, Italy
[b] Department of Mechanical and Industrial Engineering, University of Brescia, via Branze 38, I-25123 Brescia, Italy
[c] Department of Life Sciences, Cattinara University Hospital, Trieste University, Strada di Fiume 447, I-34149 Trieste, Italy

ARTICLE INFO

Keywords:
Rheology
low field NMR
Gel
Mesh size
Hydrophobic association
Thermo-sensitive

ABSTRACT

The focus of this work is on the characterization of hydrophobically-modified polyethylene glycol hydrogels, to be used as drug delivery systems, by means of the combined used of rheology and low field Nuclear Magnetic Resonance. Indeed, these two techniques allowed understanding how the transient physical bonds deriving from hydrophobic association superimpose to the pre-existing covalent bonds. We found that the improvement of physical bonds can be achieved not only by increasing the content of hydrophobic segments but also by using thermal treatments after hydrogel preparation. Moreover, we proved the reliability of an overall interpretative model linking the dependence of the shear modulus and the average magnetic relaxation time. Finally, we proposed a new mathematical approach for the determination of the magnetic relaxation spectrum. This approach reduced the computational heaviness of the procedure and allowed to easily discern the different contributes nested in the overall magnetic relaxation spectrum, an aspect that the traditional approach cannot provide directly.

1. Introduction

Hydrogels are defined as three-dimensional chemically and/or physically cross-linked hydrophilic polymeric networks that are capable of imbibing up to thousands of times their dry weight in water or biological fluids. Chemically cross-linked hydrogels feature a network of covalent bonds. In physically crosslinked hydrogels the network is formed through non-covalent interactions, e.g. hydrogen bonding, ionic interactions or hydrophobic association (Akca et al., 2020; Larrañeta et al., 2018). Their popularity was increased since the original work on synthetic crosslinked 2-Hydroxyethyl methacrylate (HEMA) hydrogels was carried out by Lim and Wichterle in the late 1950s (Wichterle and Lím, 1960). Due to their typically nontoxicity and high biocompatibility, hydrogels are particularly common in the field of life sciences and have various applications in engineering (Volpert et al., 1996, Volpert et al., 1998). Moreover, they can be manufactured with a variety of different structural features and physicochemical properties, which have been widely adopted to prepare "smart" or "intelligent" hydrogels as a depot-based drug delivery system to treat various diseases (Gupta et al., 2002; Kopecek, 2009). Indeed, hydrogels can be tailored to be sensitive to different environmental conditions, such as temperature, pH, and enzymatic activities in diseased tissues (Singh and Lee, 2014). However, despite the possibility to fine-tune hydrogels properties, there are some drawbacks which include their brittle nature (Akca et al., 2020, Miquelard-Garnier et al., 2006; Abdurrahmanoglu et al., 2009) and the modest loading capacity with hydrophobic drugs (Larrañeta et al., 2018). The first aspect depends on their very low resistance to crack propagation due to the lack of an efficient energy dissipation mechanism in the gel (Ahagon and Gent, 1975; Brown, 2007; Creton, 2017). The second regards the fact that hydrogels devoted to drug delivery have been typically designed to carry hydrophilic drugs rather than hydrophobic drugs (Pillai et al., 2014; McKenzie et al., 2015). However, the possibility of releasing hydrophobic drugs is becoming an important aspect in current pharmaceutical treatment (Gong et al., 2003; Fahr and Liu, 2007). Indeed, it is sufficient to remind that many drugs are very lipophilic since they are supposed to exert their pharmacological action at or in biological membranes/membrane-associated proteins. Poor water solubility is reported in 40% of the marketed drugs and in 60% of

* Corresponding author.
E-mail address: mario.grassi@dia.units.it (M. Grassi).

https://doi.org/10.1016/j.ijpharm.2023.122882
Received 2 December 2022; Received in revised form 17 March 2023; Accepted 19 March 2023
Available online 21 March 2023

Table 1
Composition of the feed mixtures employed in the preparations of HM hydrogels.

Sample	*f(-)*	ODA (wt%)	PEGDE (wt%)	JM600 (wt%)	JD400 (wt%)
HM_0	0	0	47.1	42.4	10.5
$HM_{0.25}$	0.25	4.8	50.2	33.8	11.2
$HM_{0.5}$	0.5	10.3	53.6	24.1	12.0
$HM_{0.75}$	0.75	16.5	57.6	13.0	12.9
HM_1	1	23.9	62.2	0	13.9

the compounds in research and development (Fahr and Liu, 2007). Different strategies were described in literature to effectively create dissipative mechanisms (Gong et al., 2003; Tanaka et al., 2005; Okumura and Ito, 2001; Haraguchi and Takehisa, 2002; Ceylan and Okay, 2007) and incorporate hydrophobic drugs within hydrogels (McKenzie et al., 2015; Fahr and Liu, 2007). Among them, hydrophobic interactions created by the incorporation of hydrophobic segments into hydrophilic polymer chains draw particular attention as these interactions provide a hydrogel with both permanent and reversible junctions with excellent mechanical performance (Gholap et al., 2004; Cram et al., 2005). Moreover, the presence of amphiphilic macromolecules highly improves the compatibility of hydrogels with hydrophobic compound (McKenzie et al., 2015). These amphiphilic polymers are usually defined as "hydrophobically-modified (HM) hydrogels". They are often block copolymers containing hydrophilic poly(ethylene glycol) (PEG) segments and hydrophobic blocks such as poly(D,L-lactide), poly(D,L-lactide-co-glycolide), or poly(ε-caprolactone) (McKenzie et al., 2015). In some cases, non-polymeric lipophilic moieties such as stearoyl, oleoyl or deoxycholic groups have been employed (Han et al., 2022; Park et al., 2020). Most of these block polymers are not chemically crosslinked. Their aqueous dispersions display a liquid or a solid-like behavior depending on concentration, temperature, pH, etc. A transition from the liquid to the solid state (sol–gel transition) is observed in these systems when the extensive association of hydrophobic groups triggers physical crosslinking.

Recently (Bignotti et al., 2021) we reported on HM hydrogels obtained by reacting amine and epoxy monomers. The hydrophilic blocks were PEG and, though to a lesser extent, poly(propylene glycol) (PPG). The hydrophobic blocks were C_{18} alkyl segments that were incorporated in the network using octadecylamine (ODA), a lipophilic amine recently used in liposomes to improve the bioavailability of poorly water-soluble drugs (Lee 2020) and in gene delivery systems to enhance their transfection ability (Vhora et al., 2018). Such systems feature both chemical and physical crosslinks. Being chemically crosslinked, contrary to common HM hydrogels, they invariably display a solid behavior in aqueous media. In our previous work we showed that, by changing the content of hydrophobic segments, it is possible to tune the extent of physical crosslinking, and consequently their mechanical properties, swelling and thermo- pH-sensitive behavior.

In this work, representing the continuation of our previous work (Bignotti et al., 2021), we investigate the fine tunability of these HM hydrogels more deeply by combining the rheological and the low field Nuclear Magnetic Resonance (LF-NMR) characterizations. Relaying on these two techniques, we could study the effect of ODA chains increase (they promote hydrophobic interactions) on both the macro (mechanical/rheological characteristics) and nano (mesh size distribution) hydrogel characteristics. Indeed, both of them are very important aspects for what concerns the hydrogel use in the drug delivery field (Grassi et al., 2007).

2. Material and methods

2.1. Hydrogel synthesis

Details on the synthesis and of the HM hydrogels were reported in Bignotti et al. (Bignotti et al., 2021). Briefly, the starting monomers were poly-(ethylene glycol)diglycidyl ether (PEGDE), Jeffamine M600 (JM600), Jeffamine D400 (JD400), and ODA. JM600 and JD400 are PPG oligomers bearing one and two terminal amino groups, respectively. The monomers were mixed at 80 °C, in the absence of solvents, then the mixture was poured into the cavities of silicone molds and crosslinked at 80 °C for 45 h. Bar-shaped specimens ($2 \times 7 \times 90$ mm^3) were obtained, which were purified by swelling in 2-propanol and finally equilibrated in NaCl 0.1 M.

By using different amounts of ODA in the feed mixture, HM hydrogels with different degrees of hydrophobicity were synthesized. The hydrophobicity of the polymeric network can be expressed using two parameters: the percentage by weight of ODA (ODA%) or the equivalent fraction *f* of ODA in the feed mixture:

$$f = eq_{ODA}/(eq_{ODA} + eq_{JM600}) \quad (1)$$

where eq_{ODA}, and eq_{JM600} are the number of aminic hydrogens deriving from ODA and JM600, respectively. Eq.(1) makes clear that the higher *f*, the higher the concentration of C_{18} alkyl segments undergoing hydrophobic association in aqueous media and consequently the expected degree of physical crosslinking. Hydrogels with five compositions were considered in this study (Table 1).

In addition, three hydrogels ($HM_{0\text{-}50}$, $HM_{24\text{-}50}$, $HM_{24\text{-}70}$) all characterized by $f = 0$, were prepared using a modified procedure. After the purification step, they were heated at 50 °C for 48 h. $HM_{0\text{-}50}$ underwent no further thermal treatment. By contrast, $HM_{24\text{-}50}$ underwent further 24 h heating at 50 °C while and $HM_{24\text{-}70}$ underwent further 24 h at 70 °C. Indeed, our aim was to evaluate the effect of ODA and temperature on hydrophobic associations. The polymer volume fraction before purification (i.e. in the crosslinking conditions) was $\nu_{p0} = 0.5$. The polymer volume fraction after purification (ν_p) (equilibrium condition – $T = 25$ °C) was evaluated relaying on the hydrogel swelling ratio (with respect to crosslinking conditions).

2.2. Rheological tests

Rheological characterization was carried out at 25 °C using an ARES G2 (TA Instrument) rheometer equipped by a parallel plate device with a diameter of 25 mm. The rheological tests were performed under oscillatory shear conditions. Strain sweep tests ensured that for all the examined samples, the linear viscoelastic range exceeded the deformation (1.3% for HM_0 and 2% for the other gels) adopted in the execution of the Frequency sweep tests, carried out in the frequency range 0.1–100 Hz. For each gel, the test was repeated three times. Frequency sweep tests were interpreted by the generalized Maxwell model as detailed in refs (Coviello et al., 2022; Staltari et al., 2022):

$$G' = G_e + \sum_{i=1}^{n} g_i \frac{(\lambda_i \omega)^2}{1 + (\lambda_i \omega)^2}; \qquad \lambda_i = \eta_i \Big/ g_i \quad (2)$$

$$G'' = \sum_{i=1}^{n} g_i \frac{\omega \lambda_i}{1 + (\lambda_i \omega)^2} \quad (3)$$

where *G*' and *G*'' are, respectively, the storage (or elastic) and the loss (or viscous) moduli, ω (=2π*f*; *f* = frequency) is pulsation and *n* is the number of the Maxwell elements considered. g_i, η_i and λ_i represent, respectively, the spring constant, the dashpot viscosity and the relaxation time of the i^{th} Maxwell element while G_e is the spring constant of the last Maxwell element which is supposed to be purely elastic. The simultaneous fitting of eq.(2) and (3) to experimental *G*' and *G*'' data was performed assuming that relaxation times (λ_i) were scaled by a factor of 10 as this approach proved to be better than letting g_i and λ_i to freely vary (Staltari et al., 2022). Based on a statistical procedure, (Draper and Smith, 1966) *n* was selected in order to minimize the product $\chi^2 * (2 + n)$, where χ^2 is the sum of the squared errors.

Starting from Flory's theory (Flory, 1953), the polymeric network

crosslink density ρ_x (defined as moles of junctions between different polymeric chains per gel unit volume) can be determined from the elastic shear modulus G (sum of all g_i plus G_e, (Pasut et al., 2008)) by:

$$G = G_e + \sum_{i=1}^{n} g_i \tag{4}$$

$$\rho_x = \left(\frac{G}{RT}\right)\left(\frac{\nu_p}{\nu_{p0}}\right)^{\frac{2}{3}} \tag{5}$$

where R is the universal gas constant, T is absolute temperature, ν_{p0} is the polymer volume fraction before purification (i.e. in the cross-linking conditions, $\nu_{p0} = 0.5$) while ν_p is the polymer volume fraction after purification.

Finally, the equivalent network theory (Schurz, 1991) allows evaluating the average network mesh size ξ according to:

$$\xi = \sqrt[3]{6/\pi\rho_x N_A} \tag{6}$$

where N_A is the Avogadro number and $(1/(N_A\rho_x))$ is the spherical volume competing to each cross-link.

2.3. LF-NMR characterization

The extinction of x-y component of the magnetization vector M_{XY} was measured by means of a Bruker Minispec MQ20 (0.47 T, 20 MHz, Germany) according to the CPMG sequence (Carr–Purcell–Meiboom–Gill) (Meiboom and Gill, 1958; Abrami et al., 2018a) sequence $\{90°[-\tau-180°-\tau(\text{echo})]_k\text{-}T_R\}$ with a 8.36 μs wide 90°pulse, $\tau = 250$ μs and T_R (recycle delay) equal to 10 s (see Supporting Information for further details on the CPMG sequence). k represents the number of experimental echoes and it is (approximately) related to the experimental test duration, T_d, by $T_d = (2\tau)*k = (2\tau)\,k'*(1 + A)$, where k' is the number of recorded echoes and A is the number of not recorded echoes. Thus, $k = k'*(1 + A)$. The try and error procedure adopted to choose k' ($\leq$1000) and A ($\leq$21) ensured that at the end of the experiment ($t = T_d$) the M_{XY} intensity (FID or $I_s(t)$) was about 2% of the initial intensity. Consequently, the time interval (T_d/k') for data acquisition is equal to $2\tau*(1 + A)$, and it can differ from sample to sample in reason of the different k' and A considered to get the desired T_d. Each relaxation experiment, composed by k' points, was repeated 36 times (four scans for each of the 9 repetitions performed on the same sample). Each sample was realized in cylindrical form in order to fit the glass tube (internal diameter 0.008 m) that could be sealed by a proper plastic top just after sample insertion. Then, the glass tube was maintained at 25 °C for, about, ten minutes before measuring. Finally, it was rapidly inserted in the MQ20 sample holder positioned just above the magnetic field.

Experimental FID reduction (indicated by $I_s(t)$) can be evaluated according to the Whittal approach (Whittal and MacKay, 1989):

$$I(t) = \int_{T_{2min}}^{T_{2max}} a(T_2)exp\left\{-\frac{t}{T_2}\right\}dT_2 \tag{7}$$

where t is time (spanning from 0 to T_d), T_2 is the spin–spin or transverse relaxation time (Brownstein and Tarr, 1979) and $I(t)$ is the theoretical FID intensity. T_{2max} (=10^4 ms) and T_{2min} (=1 ms) indicate, respectively, the lower and upper values that T_2 can assume, $a(T_2)$ is the unknown amplitude of the spectral component at the relaxation time T_2 while $\exp\{-t/T_2\}$ represents the decay term. In order to fit the experimental M_{XY} time decay ($I_s(t)$) by eq.(7), and to get the T_2 distribution (A_i-T_{2i}), where the unknowns A_i are given by the product $a_i(T_{2i})*\triangle T_{2i}$), the following discretization was applied (Whittal and MacKay, 1989):

$$I(t) \approx \sum_{i=1}^{N} a_i e^{\left\{-\frac{t}{T_{2i}}\right\}}(T_{2i+1} - T_{2i}) = \sum_{i=1}^{N} A_i e^{\left\{-\frac{t}{T_{2i}}\right\}} \tag{8}$$

where the range of the T_2 distribution ($T_{2min} - T_{2max}$) was logarithmically subdivided into $N = 200$ parts (higher N values were unnecessary). Ultimately, the adoption of eq.(8) implies the iterative determination of the N unknowns A_i, usually a heavy computational task. In order to speed up the iterative procedure, in this paper we propose a new way to determine the unknown A_i distribution. This approach consists in assuming that A_i distribution can be properly described by a sum of Weibull distributions (Tenchov and Yanev, 1986) so that eq.(8) becomes:

$$I(t) = \sum_{i=1}^{N}\left[\sum_{j=1}^{j=N_w} B_j*\left(\frac{2\delta_j}{\eta_j}\right)*\left(2\frac{T_{2i} - T_{2min-j}}{\eta_j}\right)^{\delta_j-1}*EXP\left(-\left(2\frac{T_{2i} - T_{2min-j}}{\eta_j}\right)^{\delta_j}\right)\right]e^{\left\{-\frac{t}{T_{2i}}\right\}} \tag{9}$$

where B_j, δ_j, η_j and $T_{2min\text{-}j}$ are the four fitting parameter competing to each one of the N_W Weibull distributions considered. In so doing, the fitting parameters turn out to be $4*N_W$, a much smaller unknowns number with respect to the 200 considered in eq.(8). The idea for this new approach comes from our previous findings (Turco et al., 2011; Coviello et al., 2013; Staltari et al., 2022), indicating that the sum of Weibull distributions was able to properly fit the continuous relaxation time distribution obtained by the traditional approach (eq. (8)). This, induced us to directly embody the sum of Weibull equations inside eq. (8) to get eq. (9). We have never tried to adopt other basis functions in place of the Weibull one but we feel that if the adopted distribution were not mathematically powerful, the output (distribution of relaxation times) should depend on the chosen distribution. This aspect, of course, deserves further studies. In this paper, as later on discussed, we find a perfect agreement between the traditional approach (eq. (8)) and the new one here proposed (eq. (9)). The determination of N_W was performed according to the statistical procedure (Draper and Smith 1966) described in section 2.1 (Rheology). Briefly, eq. (9) was fitted to experimental data considering only one Weibull distribution ($N_W = 1$; 4 fitting parameters) and recording the corresponding χ^2_s (see eq. (12)). Then, data fitting was repeated assuming 2 Weibull equations ($N_W = 2$, 8 fitting parameters) and recording the new value of χ^2_{s-2}. If $8*\chi^2_{s-2} < 4*\chi^2_s$, the use of two Weibull equations was statistically necessary. This procedure stopped when $(4*N_W)*\chi^2_{s-N_W} \geq (4*(N_W\text{-}1))*\chi^2_{s-N_W-1}$.

On the basis of eq. (8), the average relaxation time (T_{2m}) and the average value of the relaxation time inverse ($(1/T_2)_m$) can be defined by:

$$T_{2m} = \sum_{i=1}^{N} A_i T_{2i} \Big/ \sum_{i=1}^{N} A_i; \qquad \left(\frac{1}{T_2}\right)_m = \sum_{i=1}^{N} \frac{A_i}{T_{2i}} \Big/ \sum_{i=1}^{N} A_i \tag{10}$$

The percentage fraction ($A_{i\%}$) of dipoles relaxing with the relaxation time T_{2i} can be evaluated by:

$$A_{i\%} = 100A_i / \sum_{i=1}^{N} A_i \tag{11}$$

Because of the noise disturbing the measure of I_s, the fitting procedure must not minimize the χ^2 statistic, but a smoothed definition

Table 2
Dependence of the average tanδ value with the ODA equivalent fraction *f* referring to the data shown in Fig. 1. *r* is the Pearson correlation coefficient.

Sample	*f*(-)	tanδ ± SD	Pearson correlation coefficient
HM_0	0	$(5.2 \pm 5.7)*10^{-3}$	$r = 0.997$, $p = 10^{-4}$
$HM_{0.25}$	0.25	0.16 ± 0.035	**Linear interpolant**
$HM_{0.5}$	0.5	0.26 ± 0.054	
$HM_{0.75}$	0.75	0.39 ± 0.11	**tan**δ = (0.51 ± 0.02)**f* + (0.015 ± 0.012)
HM_1	1	0.53 ± 0.14	

(Whittal and MacKay, 1989) of it (χ_s^2):

$$\chi_s^2 = \sum_{i=1}^{N}\left(\frac{I_s(t_i) - I(t_i)}{\sigma_i}\right)^2 + \mu\sum_{i=1}^{N-2}|A_{i+2} - 2A_{i+1} + A_i|^2 \quad (12)$$

where σ_i is the i^{th} datum standard deviation, μ is the weight of the smoothing term (second summation in eq. (12)) proposed by Provencher (Provencher, 1982). Although different criteria can be used to determine μ, the strategy proposed by Wang (Wang and Ni, 2003) was applied. Based on this strategy, the correct μ value is that occurring just below the heel (slope variation) of the function $\ln(\chi_s)$ vs $\ln(\mu)$. In this work, $\mu = 150$ was determined.

The T_2 distribution can be transformed into hydrogel mesh size distribution resorting to one of the fundamental relations of the low-field NMR field. This relation, based on the solution of the magnetization diffusion equation proposed by Brownstein and Tarr (Brownstein and Tarr, 1979), establishes the link between $(1/T_2)_m$ and the ratio of the surface (*S*) of the dispersed/solubilized substances in the sample and the volume (*V*) of the sample water molecules:

$$\left(\frac{1}{T_2}\right)_m = \frac{1}{T_{2H2O}} + \frac{S}{V}\mathscr{M} = \frac{1}{T_{2H2O}} + \mathscr{M}\frac{2}{\xi\sqrt{\frac{C_0}{C_1}\frac{1-0.58\nu_p}{\nu_p}}} \quad (13)$$

where T_{2H2O} is the bulk protons relaxation time (i.e. the water proton relaxation time in the absence of polymer, the so-called free water relaxation time (see Appendix)), C_0 and C_1 are two constants depending on mesh size architecture ($C_0 = 1$ and $C_1 = 3\pi$ for a cubical network) while $\mathscr{M}$ (length/time) is a physical parameter, named relaxivity. It represents the effect of the polymer chains surface on water protons relaxation being the ratio between the thickness and the relaxation time of the bound water layer adhering to the solid surface. Eq.(13), stating that $(1/T_2)_m$ depends on (*S*/*V*), clearly establishes the relation between the relaxation time and the spatial organization of the sample network that heavily affects the *S*/*V* ratio (Chui et al., 1995). Usually, in polymeric solutions, crosslinking induces a spatial reorganization of the polymeric chains that involves the increase of the ratio *S*/*V* (Abrami et al., 2019a; Kopač et al., 2022). This, in turn, reflects in the increase of $(1/T_2)_m$ and in the decrease of T_{2m}.

As the Fiber-Cell (Chui et al., 1995) and the Scherer (Scherer, 1994) theories allow to express the ratio (*S*/*V*) as a function of ν_p and ξ (see the third term in eq.(13)), eq.(13) permits to get a direct relation between mesh size and relaxation time (Abrami et al., 2018b; Mezzasalma et al., 2022):

$$\xi_i = \xi\frac{\left(\left(\frac{1}{T_2}\right)_m - \frac{1}{T_{2H2O}}\right)}{\left(\frac{1}{T_{2i}} - \frac{1}{T_{2H2O}}\right)} \quad (14)$$

where T_{2i} is the relaxation time of water protons trapped inside meshes of size ξ_i.

Thus, eq.(8) or eq.(9) fitting to experimental M_{XY} decay ($I_s(t)$) allows determining the relaxation spectrum ($A_{i\%}$ - T_{2i}), whereas eq.(14) allows the conversion of the time relaxation spectrum into the mesh size relaxation spectrum ($A_{i\%}$ - ξ_i). Notably, eq.(14) rigorously holds only in the fast-diffusion regime, i.e. when the mobility of water molecules, expressed by their self-diffusion coefficient *D*, is large as compared to the rate of magnetization loss, identifiable with (R_c*$\mathscr{M}$), i.e., R_c*$\mathscr{M}/D \ll 1$, where R_c is defined by (Chui et al., 1995):

$$R_c = \frac{R_f}{\sqrt{\nu_p}} \quad (15)$$

being R_f the radius of the polymeric chain assumed to be a long cylinder. Due to the typical values of R_c (order of magnitude 10^{-8} m), *D* (order of magnitude 10^{-9} m^2/s at 25 °C (Holz et al., 2000)) and $\mathscr{M}$ (order of magnitude $10^{-5} - 10^{-8}$ m/s) (Kopač et al., 2022, De'Nobili et al., 2015; Halib et al., 2014), fast-diffusion regime is always well attained in the case of hydrogels.

2.3.1. *Water self-diffusion coefficient*

In order to study water mobility inside the gel network, pulsed gradient spin echo (PGSE - see "Supporting information" for further details on this sequence) measurements were performed at 25 °C. The applied sequence consisted in the classical echo sequence with two equal gradient pulses (of length $\delta_m = 1$ ms) occurring at $x_1 = 1$ ms and $x_2 = 1$ ms after the 90 and 180° pulses, respectively. The time separation, indicated by △ (≈ τ-x_1 - δ_m + x_2), is related to the water molecule diffusion time (t_d) according to $t_d = (\triangle - \delta_m/3)$. The determination of the moving species self-diffusion coefficient was led fitting the following equation to experimental data (Skirda et al., 1999):

$$A_t = \sum_{i=1}^{N_p} A_{0i}e^{-q^2 t_d D_{wi}}; \qquad q = \gamma g \delta_m; \qquad A_0 = \sum_{i=1}^{p} A_{0i} \quad (16)$$

where A_t and A_0 are, respectively, the measured amplitude of the signal at the echo with and without applied gradient, γ is the proton gyromagnetic ratio, *g* is the known magnetic field gradient while A_{0i} are the fractions of protons characterized by a self-diffusion coefficient D_{wi}. In the case of a homogeneous system, of course, the summation limits to the first term ($p = 1$) as all the protons are characterized by the same self-diffusion coefficient. Also in this case, N_p was determined minimizing the product χ^2 *$2N_p$ where χ^2 is the sum of the squared errors and $2N_p$ represents the number of fitting parameters (A_{0i}, D_{wi}) of eq.(16) (Draper and Smith, 1966).

Finally, network tortuosity, τ_o, could be evaluated as the ratio between the average water self-diffusion coefficient inside the network and the free water self-diffusion coefficient at 25 °C ($D_{H2O} \approx 2.30*10^{-9}$ m^2/s (Holz et al., 2000)) (Latour et al., 1993; Latour et al., 1995).

3. Results

Fig. 1-A shows that when ODA is absent, sample HM_0 is characterized by an evident gel behavior as *G*' and *G*'' are pulsation (ω) independent and *G*' is more than two orders of magnitude higher than *G*''. Consequently, the average value of tanδ (=*G*''/*G*') is statistically equal to zero ($(5.2 \pm 5.7)*10^{-3}$).

The increase of ODA equivalent fraction (*f*) clearly implies the increase of both *G*' and *G*'' with a more marked effect on *G*'' as proved by the increase of the average tanδ values (see Table 2). Interestingly, this increase is linearly correlated with *f*, being the Pearson correlation coefficient close to one (see Table 2). This behavior can be explained remembering that as hydrophobic interactions do not give origin to permanent chemical crosslinks but to labile transient bonds, statistically speaking, on average, only a fraction of them works as elastic connectors determining the *G*' increase (Lapasin and Pricl, 1995). On the contrary, the complementary fraction should be associated to dissipative mechanisms promoting *G*'' increase. Thus, *G*' increase witnesses the simultaneous increase of chemical and statistically permanent physical crosslinks (reflecting the increase of the overall crosslink density and the decrease of the average mesh size see Table 3). On the contrary, *G*'' increases indicates the increase of physical interactions among chains that cannot give origin to elastically active "zones", but interaction "zones" allowing a hindered, relative motion of interacting chains (or portion of chains). The increase of tanδ implies that ODA increase

Table 3
Parameters relative to the generalized Maxwell model (eq.(2) and (3)) best fitting to the experimental data shown in Fig. 1A, B, C. G_e and g_i, are the spring constants while λ_1 is the relaxation time of the first Maxwell element. G is the shear modulus, ρ_x is the crosslink density, ν_p is the polymer volume fraction and ξ is the average mesh size of the polymer network. F_{test} indicates the result of the F statistic test relative to each data fitting.

	HM_0	**$HM_{0.25}$**	**$HM_{0.5}$**	**$HM_{0.75}$**	**HM_1**
λ_1(s)	$(2.5 \pm 1.6)*10^{-3}$	$(1.6 \pm 0.09)*10^{-3}$	$(1.2 \pm 0.08)*10^{-2}$	$(1.2 \pm 0.08)*10^{-2}$	$(1.4 \pm 0.1)*10^{-2}$
G_e (Pa)	899 ± 238	5133 ± 425	12558 ± 414	11268 ± 388	22765 ± 275
g_1 (Pa)	76 ± 43	2956 ± 184	13974 ± 504	28464 ± 1233	133937 ± 5958
g_2 (Pa)	–	2879 ± 116	13529 ± 423	28460 ± 1000	106941 ± 4229
g_3 (Pa)	2.76 ± 2.65	1325 ± 62	7438 ± 356	20571 ± 898	24125 ± 1803
g_4 (Pa)	6.1 ± 2.1	208 ± 14	1103 ± 82.3	4230 ± 313	3264 ± 313
G (Pa)	984 ± 242	12503 ± 481	48123 ± 859	92993 ± 1891	92993 ± 212
F_{test}	$F(6,25,0.95) < 28.5$	$F(6,25,0.95) < 984$	$F(6,25,0.95) < 1139$	$F(6,25,0.95) < 721$	$F(6,25,0.95) < 2907$
ν_p(-)	0.038	0.104	0.193	0.252	0.365
ρ_x (mol/cm^3)	$(7.1 \pm 1.7)*10^{-8}$	$(1.7 \pm 0.07)*10^{-6}$	$(1.0 \pm 0.02)*10^{-5}$	$(2.4 \pm 0.05)*10^{-5}$	$(9.5 \pm 0.15)*10^{-5}$
ξ (nm)	35.4 ± 2.9	12.1 ± 0.16	6.7 ± 0.04	5.1 ± 0.04	3.2 ± 0.03
$HM_{0\text{-}50}$					
λ_1(s)	$(9.0 \pm 0.6)*10^{-3}$				
G_e (Pa)	5239 ± 2053				
g_1 (Pa)	130 ± 7				
g_2 (Pa)	196 ± 6				
g_3 (Pa)	85 ± 3				
g_4 (Pa)	90 ± 10				
G (Pa)	6000 ± 2053				
F_{test}	$F(6,25,0.95) < 164$				
ν_p(-)	0.079				
ρ_x (mol/cm^3)	$(7.1 \pm 2.4)*10^{-7}$				
ξ (nm)	16.5 ± 2.0				

preferentially promotes the growth of these labile interaction zones.

Fig. 1A and B clearly indicate that the generalized Maxwell model (eq.(2) and (3)) can properly fit our experimental data (as also proved by the F_{test} – see Table 3) and it allows to evaluate the shear modulus (G – eq.(4)), the crosslink density (ρ_x – eq.(5)) and the average mesh size (ξ – eq.(6)) as reported in Table 3. The inspection of Table 3 reveals that four Maxwell elements are needed to fit our experimental data and that the shear modulus (G) increases with ODA equivalent fraction (f). Consequently, f increase reflects in the reduction of the average mesh size ξ that undergoes an order of magnitude reduction passing from $f = 1$ to $f = 0$.

Fig. 1C, showing the mechanical spectrum referring to the $HM_{0\text{-}50}$ sample, indicates that heating implies a considerable increase of both G' and G'' with respect to the "native" HM_0 sample (Fig. 1A) that did not undergo heating. Interestingly, however, the increase of G' is more pronounced than the G'' one as also proved by the small value of tanδ ($(15.4 \pm 2.7)*10^{-3}$). Thus, the effect of heating is not completely equivalent to the effect of ODA increase. However, also in the case, $HM_{0\text{-}50}$ sample shows the typical behavior of a strong gel and the generalized Maxwell model.

(eq.(2) and eq.(3)) proved to properly fit its mechanical spectrum (solid lines in Fig. 1C) as also witnessed by the F_{test} score (see Table 3).

While LF-NMR represents a powerful tool to study the spatial organization of solid substances (polymeric chains, in our case) in a hydrogenated liquid, it is essential to know the relaxation of which hydrogens we are following, i.e. those of the polymeric chains or those of the hydrogenated liquid (water, in our case). Indeed, as far as we know, two main approaches exist in literature to characterize the structure of a polymeric network by means of LF-NMR.

The first one is that looking at the relaxation of polymer chains hydrogens (Saalwachter, 2003; Mauri et al., 2008; Saalwachter et al., 2013), while the second one focusses on the relaxation of water hydrogens trapped inside the network (Brownstein and Tarr, 1979; Chui et al., 1995; Scherer, 1994). In the light of our expertise/equipment, we pursued the second characterization strategy. Thus, we conceived an experiment implying hydrogels immersion in deuterated water (D_2O) for increasing times. Due to the substitution of the H_2O molecules contained in hydrogel by the external D_2O, the initial FID intensity has to decrease with immersion time as we cannot detect the D_2O signal being characterized by a very different Larmor frequency with respect to 1H. Thus, after a sufficient long immersion time, FID intensity should go to zero unless we record also the relaxation of hydrogens belonging to polymer chains. Accordingly, we evaluated the ratio R between FID intensity after different immersion times and FID intensity before immersion as depicted in Fig. 2 for different systems. It is evident that R decreases for all the considered systems and, after 96 h immersion, it gets zero. This evidence witnesses that, in our experimental setup, we could follow only the relaxation of the water hydrogens. The fact that, at the beginning, R is not 100 for all systems is simply due to different signal amplification adopted for the different systems in order to optimize each measurement. Similarly to what seen for the rheological characterization, also LF-NMR is able to detect the effect of f increase as depicted in Fig. 3. Indeed, it can be seen that f increase reflects in a faster and faster relaxation process that takes, about, 10^4 ms when $f = 0$ while it decreases of more than one order of magnitude when $f = 1$.

This behavior simply indicates that f increase implies a variation of the S/V ratio, this being connected to a variation of the hydrogel nanostructure as found by means of the rheological characterization. In addition, it can be seen that eq.(8) (solid lines of Fig. 3) is able to perfectly fit the experimental data whatever the f value (circles in Fig. 3). In order to get deeper information from the LF-NMR characterization, Fig. 4 reports the outcomes of eq.(8) and (9) best fitting in terms of relaxation spectrum ($A_{i\%}$ vs T_{2i}) referring to system HM_0. Firstly, it is worth underlying that the relaxation spectrum deriving from eq.(8) (circles of Fig. 4) is practically coincident with that competing to eq.(9) considering two Weibull equations (solid line of Fig. 4) as suggested by the statistically procedure explained in section 2.3. Notably, this perfect agreement was found for all the studied systems, thus proving the reliability of the hypothesis on which eq.(9) relies, i.e. the possibility to describe the magnetic relaxation spectrum as the sum of one, or more, Weibull equations. This represents a considerable advantage since the use of eq.(9) not only allows to speed up a lot the fitting procedure, but it permits also to immediately discern the different contributes nested in the overall magnetic relaxation spectrum (solid line in Fig. 4), an aspect that eq.(8) cannot provide.

Indeed, it is evident that the magnetic relaxation spectrum exceeds 3634 ms, the maximum relaxation time of free water at 25 °C and 20 MHz (see Appendix for further considerations on the free water

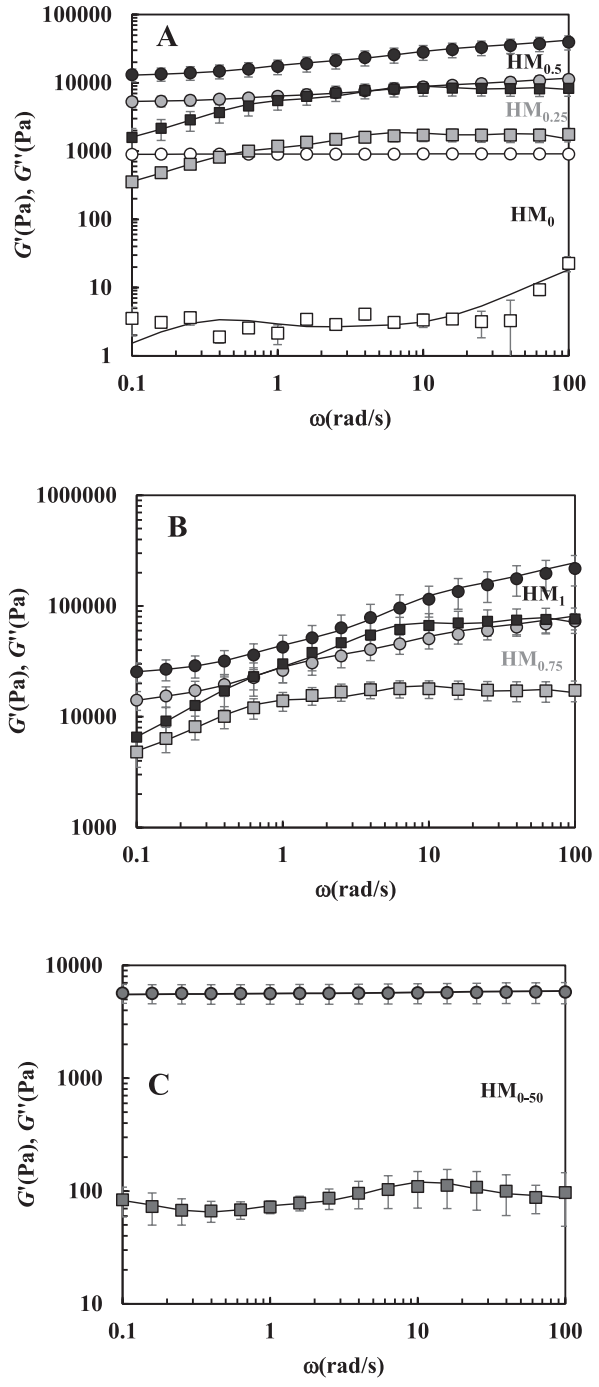

Fig. 1. Mechanical spectra referring to **A)** hydrogels HM_0, $HM_{0.25}$, $HM_{0.5}$**B)** $HM_{0.75}$, HM_1 and **C)** $HM_{0\text{-}50}$. While ω indicates pulsation, elastic (*G*') and viscous (*G*'') moduli are represented by circles and squares, respectively. Solid lines show the generalized Maxwell model best fitting (eq.(2)-(3)) and vertical bars indicate datum standard error.

relaxation time T_{2H2O}). This apparent paradox can be explained supposing that part of the water present in system HM_0 is embedded in the polymeric network (81% in volume, dashed line – first Weibull) while the other part is external to the network (19%, dotted line – second Weibull) (see Fig. 4). The reasonability of this statement is proved by the position and the wideness of the two peaks (dashed and dotted line in Fig. 4). The peak associated to the outer, or, free water (dotted line) spans in the range 2200 – 4400 ms, i.e. a range very similar to that of free

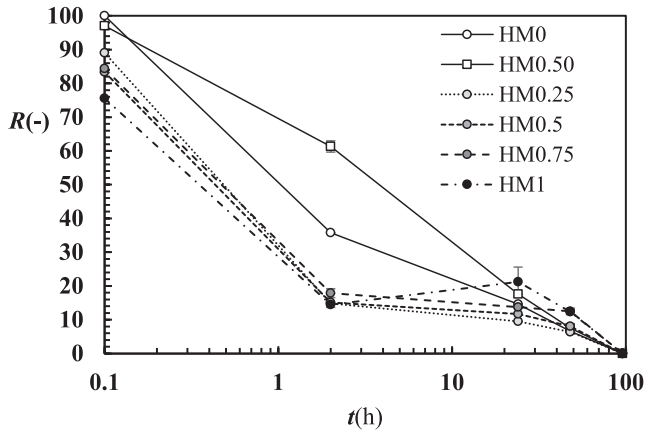

Fig. 2. Reduction of the ratio *R* between FID intensity at $t = 0$ and after sample immersion in deuterated water up to time *t*.

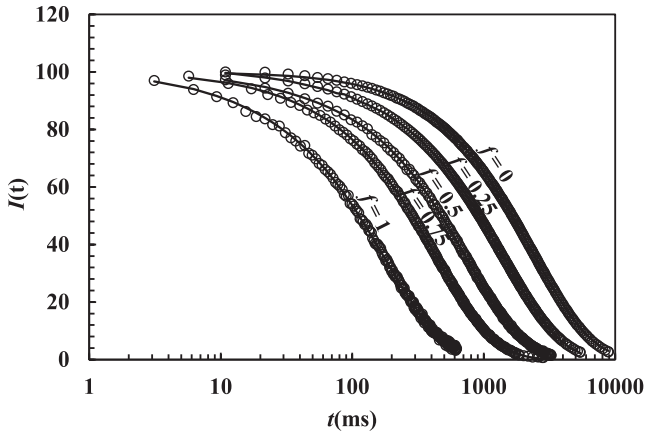

Fig. 3. FID reduction (*I*(*t*)) referring to hydrogels HM_0 ($f = 0$), $HM_{0.25}$, ($f = 0.25$), $HM_{0.5}$, ($f = 0.25$), $HM_{0.75}$ ($f = 0.75$) and HM_1 ($f = 1$). Circles indicate experimental data while solid lines represent eq. (8) best fitting.

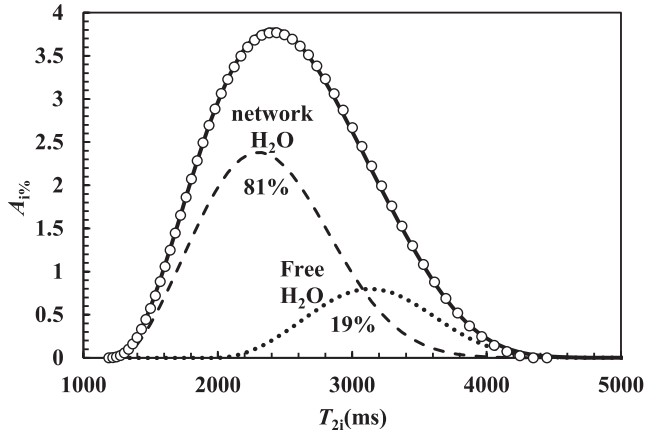

Fig. 4. Magnetic relaxation spectrum ($A_{i\%}$ vs T_{2i}) referring to sample HM_0 ($f = 0$) and descending from the use of eq. (8), circles, and eq. (9), solid line. Dashed and dotted lines represent, respectively, the water contained inside (81% in volume) and outside (19% in volume) the polymeric network.

water (see Appendix). In all other hydrogels, the presence of external water was not detected as shown in Fig. 5. Indeed, the position of the two peaks characterizing the magnetic relaxation spectra of hydrogels characterized by $f > 0$, is well below that of the free water one (around

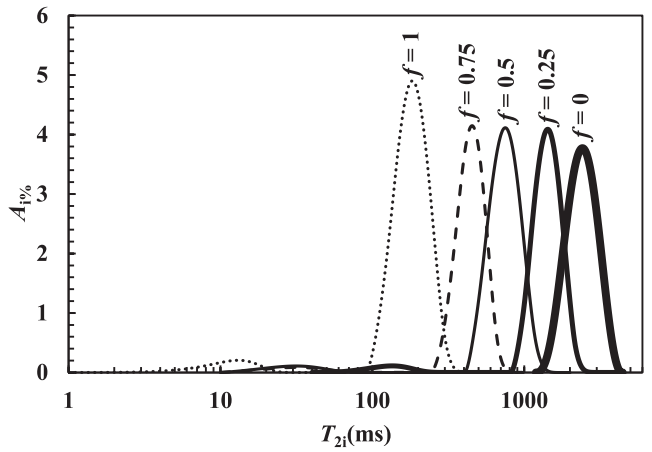

Fig. 5. Magnetic relaxation spectrum ($A_{i\%}$ vs T_{2i}) referring to the samples characterized by different equivalent ODA fraction: HM_0 ($f = 0$), $HM_{0.25}$, ($f = 0.25$), $HM_{0.5}$, ($f = 0.25$), $HM_{0.75}$ ($f = 0.75$) and HM_1 ($f = 1$).

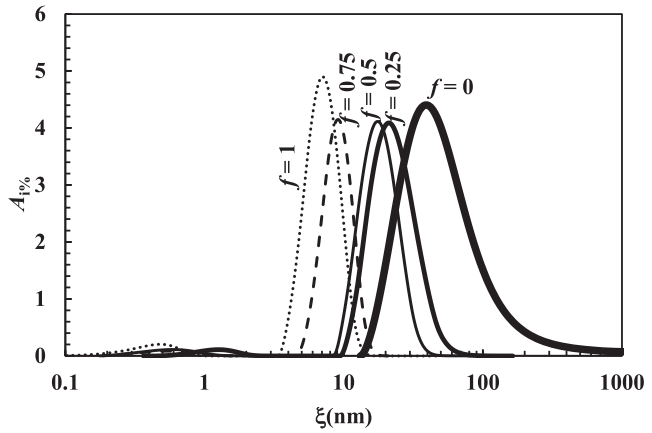

Fig. 6. Mesh size distribution ($A_{i\%}$ vs ξ) referring to the samples characterized by different equivalent ODA fraction: HM_0 ($f = 0$), $HM_{0.25}$, ($f = 0.25$), $HM_{0.5}$, ($f = 0.25$), $HM_{0.75}$ ($f = 0.75$) and HM_1 ($f = 1$).

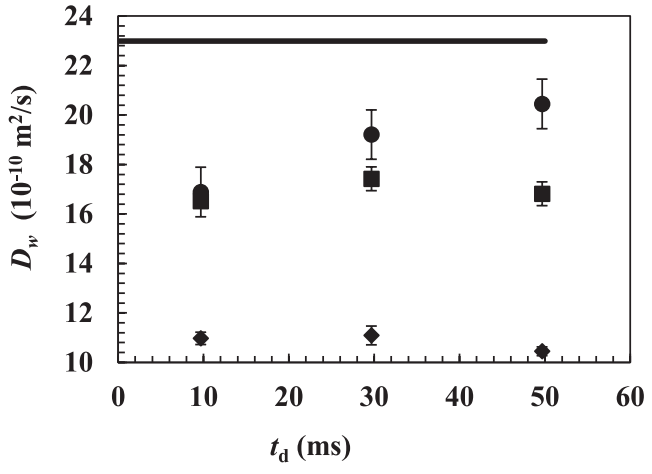

Fig. 7. Water self-diffusion coefficient (D_w) vs the diffusion time (t_d) referring to hydrogels HM_0 (circles), $HM_{0.5}$ (squares) and HM_1 (diamond). Solid line indicates the free-water self-diffusion coefficient (25 °C, 20 MHz) while vertical bars indicate standard deviation.

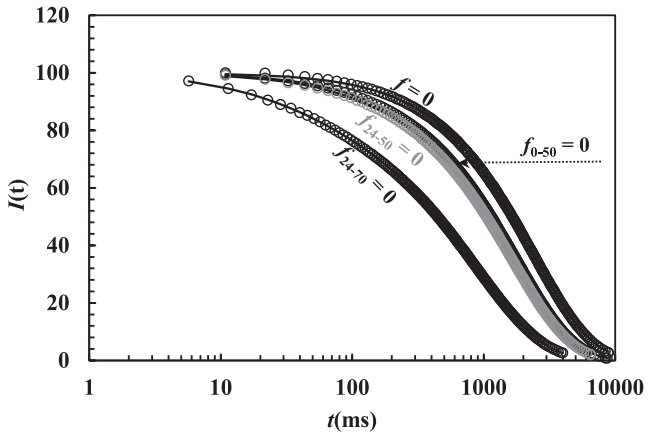

Fig. 8. FID reduction ($I(t)$) referring to hydrogels HM_0 ($f = 0$), $HM_{0\text{-}50}$, ($f = 0$), $HM_{24\text{-}50}$, ($f = 0$) and $HM_{24\text{-}70}$ ($f = 0$). Circles indicate experimental data while solid lines represent eq. (8) best fitting.

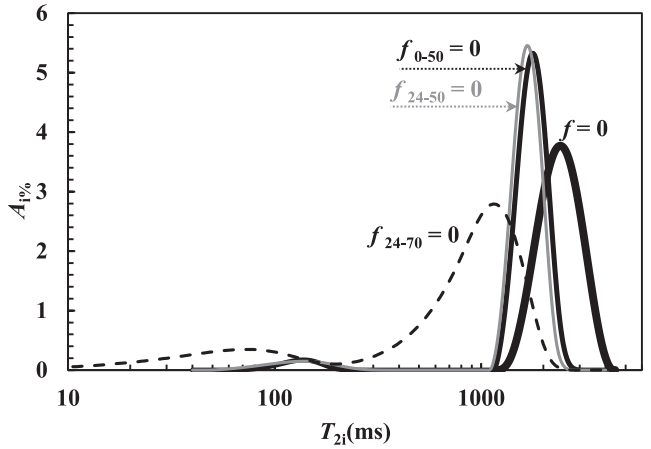

Fig. 9. Magnetic relaxation spectrum ($A_{i\%}$ vs T_{2i}) referring to the samples characterized by different thermal treatment and the absence of ODA ($f = 0$): HM_0, $HM_{0\text{-}50}$, $HM_{24\text{-}50}$, and $HM_{24\text{-}70}$.

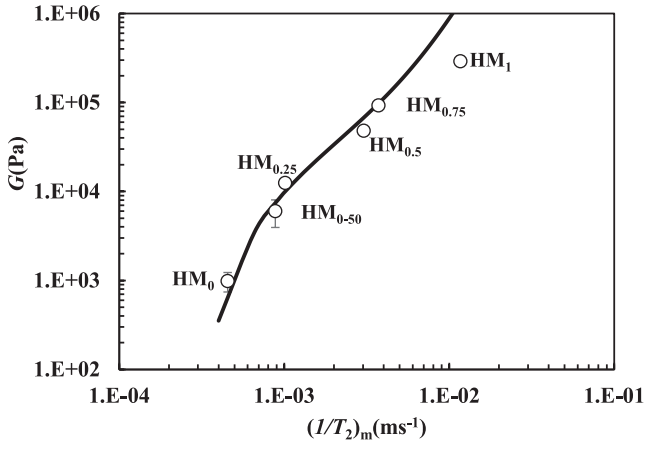

Fig. 10. Experimental (circles) and theoretical (solid line, eq.(17) fitting) relation existing between the shear modulus G and the average value of the inverse of the relaxation time ($(1/T_2)_m$) for the studied hydrogels. Vertical bars indicate data standard error. ($HM_{0\text{-}50}$: $G = 6000$ Pa, $\nu_p = 0.0793$; $(1/T_2)_m = 8.83{*}10^{-4}$ ms^{-1}).

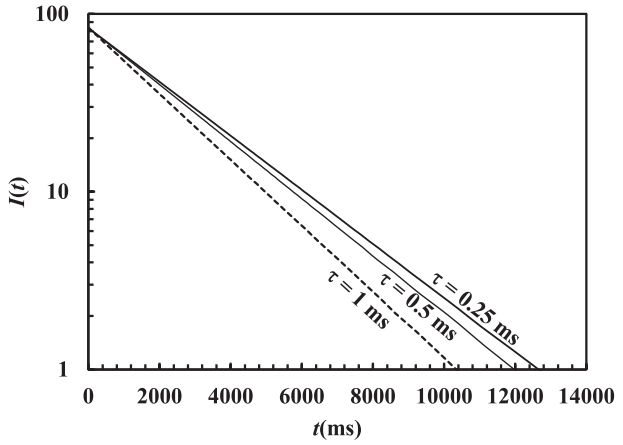

Fig. A1. FID ($I(t)$) decay dependence on the time separation τ between the 90 and 180 pulses of the CPMG sequence in the case of Milli-Q water at 25 °C and 20 MHz.

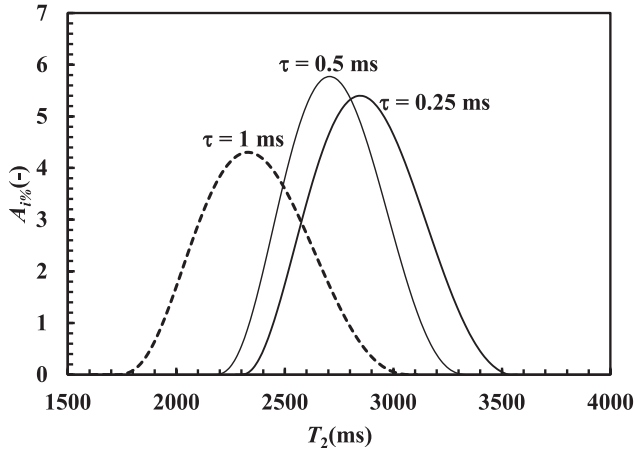

Fig. A2. Relaxation spectra corresponding to the three decay curves depicted in Fig. A1.

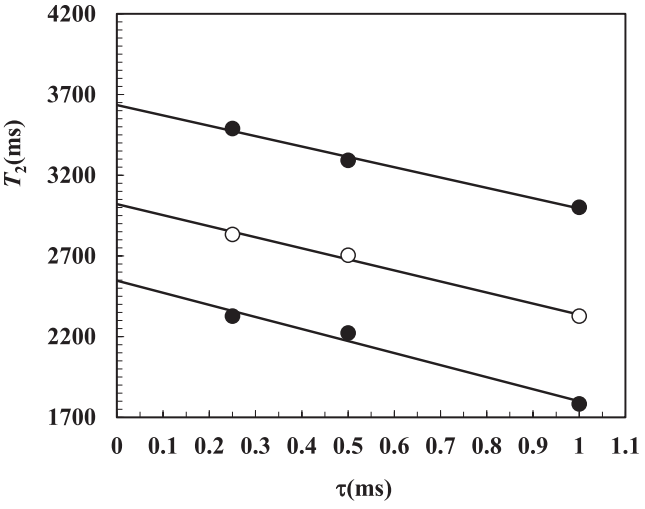

Fig. A3. Effect of τ increase on the displacement of the peak (white circles) and the two extremes (black circles) competing to the three distributions reported in Fig. A2. Solid lines represent the linear interpolants.

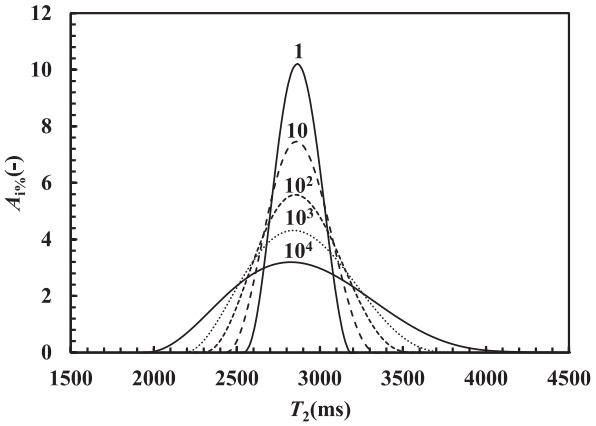

Fig. A4. Effect of smoothing factor increase (μ = 1, 10, 10^2, 10^3 and 10^4) on the water relaxation time distribution (lines) fixing τ = 0.25 ms, 25 °C and 20 MHz.

3000 ms – see Appendix). Interestingly, f increase implies the shifting of both peaks towards smaller relaxation times, this witnessing a change in the S/V ratio that, in turn, is connected to a variation of the network architecture (see eq. (13)). In addition, the appearance of the second peak indicates the formation of a heterogeneous structure where two main families of relaxing hydrogens can be found.

As in the pivot hydrogel (HM_0, $f = 0$) the second peak is not present, we have to conclude that hydrophobic interactions promote also a moderate (the second peak represents about 4%-6%) heterogeneity of the polymeric network.

Relaying on eq. (14), it is possible giving a more precise physical meaning to these considerations. Indeed, eq. (14) allows converting the magnetic relaxation spectrum reported in Fig. 5 into the corresponding mesh size distributions shown in Fig. 6. Looking at Fig. 6, the effect of f variation can be interpreted as the reduction of the network mesh size and the formation of "big" (those competing to the most evident peak) and "small" (those competing to the smaller peak) meshes. The description of the network three-dimensional organization can be furtherly enriched by evaluating the water self-diffusion coefficient (D_w) in three representative hydrogels, i.e. HM_0, $HM_{0.5}$ and HM_1. Fig. 7 shows that whatever t_d, D_w is substantially constant for all the three hydrogels, this simply implying that all the meshes are interconnected, i.e. there are not network zones that cannot be accessed by water molecules. Indeed, should the majority of the meshes be not interconnected, D_w will continuously decrease with t_d (Latour et al., 1995). This finding is also supported by Fig. 2 showing that D_2O molecules have access to all the network meshes. Indeed, they can completely replace all the H_2O molecules. In addition, eq. (16) fitting to the experimental data (A_t/A_0 vs q^2 – see supporting information) reveals that only one principal diffusion mode exists inside the network ($N_p = 1$; water), i.e. the diffusion of our molecular probe (water molecules) is equally hindered whatever its position in the network.

This means that our probe is diffusing in a homogeneous environment, a conclusion that is not in contrast with the network heterogeneity revealed by relaxation data (Figs. 5 and 6). Indeed, as previously noticed, the heterogeneous zones represent a small fraction (4%-6%) of the whole hydrogel volume. Coherently, however, the higher f, the lower D_w, this translating in an increased network tortuosity with f ($\tau_{o\text{-}HM0} = 1.22$; $\tau_{o\text{-}HM0.5} = 1.36$ and $\tau_{o\text{-}HM1} = 2.12$). This conclusion perfectly agrees with the reduction of mesh size with f determined by means of the rheological and LF-NMR characterization previously discussed.

Once the effect of ODA equivalent fraction (f) increase on the polymeric network topology has been clarified, it is interesting to look at the effect of the thermal treatment on the network connectivity. At this purpose, three additional hydrogels were considered. The first consisted in the pivot hydrogel (HM_0) that was heated at 50 °C ($HM_{0\text{-}50}$) for 48 h

after purification, the second underwent further 24 h hours heating at 50 °C ($HM_{24\text{-}50}$) and the last underwent additional 24 h heating at 70 °C ($HM_{24\text{-}70}$). The effect of the different thermal treatment is reported in Fig. 8 where the FID decay referring to these three systems is depicted. It is clear that the more intense the thermal treatment, the faster the magnetic relaxation process.

Also in the case of these new hydrogels, eq. (8) and eq. (9) best fitting to FID reduction provided identical results and the same magnetic relaxation spectrum. In addition, Fig. 9 stresses the similitude existing between the effect of the thermal treatment and the *f* increase.

Thus, the thermal treatment plays an effect not dissimilar to that played by *f* increase, i.e. it favours the hydrophobic interactions whose increase leads to a more interconnected network. It is interesting to remember that the thermal treatment caused hydrogel shrinking so that the LF-NMR characterization was performed after the removal of the expelled water. Indeed, also the thermal treatment gives origin to a two peaks magnetic relaxation spectrum whatever the thermally treated hydrogel considered. Moreover, the improvement of the thermal treatment implies the shifting of both peaks towards smaller relaxation times, similarly to what observed in the case of *f* increase. It is worth evidencing that when $f = 0$, no C18 hydrophobic segments are present, but only PPG and PEG blocks. Concentrated aqueous solutions of PEG-PPG-PEG triblock copolymers, known as poloxamers, display a liquid behavior at low temperature but form a gel when heated above a critical temperature, due to the aggregation of individual chains, formation of micelles and eventually of a three-dimensional physical network (Rey-Rico and Cucchiarini, 2018). This aggregation occurs because the PPG blocks progressively become dehydrated and less soluble as the temperature increases (Grinberg et al., 2018). Therefore, the effect of thermal treatment observed in the hydrogels with $f = 0$ can be explained by assuming that at room temperature the PPG blocks are hydrated and not prone to hydrophobic association.

However, when these hydrogels are heated at 50°-70 °C, the PPG segments lose their hydration water and undergo extensive hydrophobic association, resulting in a magnetic relaxation spectrum shifted towards smaller times. A second effect of heating is the reduction of the volume, and consequently of the water content. As highlighted by Bignotti and co-workers (Bignotti et al., 2021), if *f* increases, the water content of HM hydrogels decreases. Therefore, an increase in temperature or *f* causes a volume reduction in both cases as physical crosslinks are increased. It is well-known that the higher the crosslink density of a polymeric network the lower its tendency to expand due to water absorption.

It is also interesting performing a check on the combined use of rheology and LF-NMR. At this purpose, combining eq.(4)-(6) and eq.(13) it is possible expressing the shear modulus (*G*) dependence on $((1/T_2)_m)$:

$$G = \frac{3}{4}\frac{RT}{\pi N_A}\left(\frac{\nu_{p0}}{\nu_p}\right)^{\frac{2}{3}}\left[\frac{\left(\left(\frac{1}{T_2}\right)_m - \frac{1}{T_{2H2O}}\right)\sqrt{\frac{1-0.58\nu_p}{3\pi\nu_p}}}{\mathscr{M}}\right]^3 \quad (17)$$

where the only fitting parameter is the relaxivity $\mathscr{M}$. Eq.(17) fitting to experimental data depicted in Fig. 10 is statistically reliable ($F(1,5,0.95) < 21$) and yields to $\mathscr{M} = (5.34 \pm 0.2)*10^{-9}$ m/s. This value is a little bit smaller with respect to those characterizing other polymeric systems (10^{-5} –10^{-8} m/s) (Kopač et al., 2022; De'Nobili et al., 2015; Halib et al., 2014). However, it is well known that $\mathscr{M}$ is strictly dependent on the polymer surface chemistry and this is the first attempt to evaluate $\mathscr{M}$ for these polymers. The internal consistency of the LF-NMR/Rheology approach represents a very encouraging and strong point for the reliability of mesh size evaluation according to eq.(14). Indeed, as nicely documented by Amsden (Amsden 1998; Amsden 2022), a precise knowledge of mesh size is essential for the determination of the drug diffusion coefficient inside a polymeric network. Diffusion coefficient, in turn, highly affects the drug release kinetics when diffusion is the leading mass transport phenomenon (Grassi et al 2007). Interestingly, although much more complex situations could be considered, Abrami and co-workers (Abrami et al, 2019b) proposed a simple, but meaningful way to establish a direct connection between the mesh size distribution from eq.(14) and the drug diffusion coefficient inside a polymeric network.

4. Conclusions

In this work we demonstrated the potentiality of the combined used of rheology and LF-NMR for the characterization of hydrophobically-modified PEG hydrogels. Indeed, these two techniques allowed understanding how the transient physical bonds deriving from hydrophobic association superimpose to the pre-existing covalent bonds. Interestingly, we found that the improvement of physical bonds is not only due by an increase of the content of hydrophobic segments but also by more intense thermal treatments that determine the shrinking of the previously formed hydrogel. However, the rheological characterization reveals that thermal treatment and ODA increase are not perfectly equivalent as the thermal treatment seems to be more efficient in increasing network elasticity. All in all, these are a very important aspects as the combination of network hydrophobicity and thermal treatment allow to fine-tune hydrogel properties in term of mesh size and interaction with hydrophobic drugs, whose loading in hydrogel, usually, is not an easy task. Moreover, it was possible to determine not only the gels macroscopic properties (mechanical and magnetic relaxation spectra) but also their nanoscopic properties via the determination of the mesh size distribution, a very important aspect for all the hydrogels devoted to controlled drug delivery (Abrami et al., 2019a). Interestingly, we also proved the reliability of the overall interpretative model represented by eq. (17) despite the numerous simplifying hypotheses connected to the theoretical interpretation of the rheological and LF-NMR data. Thus, at least for our hydrogels, we can conclude that *G* and ξ could be also evaluated on the basis of the magnetic relaxation spectrum of water molecules trapped in the network meshes. However, we feel that eq. (17) should not hold when structurally complex polymeric networks, characterized by the presence of pendant chains, branches, loops and so on, are considered. Indeed, in these cases, the approximation of polymer chains by long cylinders (as requested by the Fiber-cell and Scherer theories) does not seem reliable.

Finally, we propose a new mathematical approach for the determination of the magnetic relaxation spectrum. This approach not only reduces a lot the computational heaviness of the procedure, but it allows also to easily discern the different contributes nested in the overall magnetic relaxation spectrum, an aspect that the traditional approach cannot provide.

CRediT authorship contribution statement

Michela Abrami: Conceptualization, Investigation, Methodology, Writing – original draft. **Fabio Bignotti:** Conceptualization, Investigation, Methodology. **Francesco Baldi:** Formal analysis, Writing – review & editing. **Gloria Spagnoli:** Investigation. **Alice Biasin:** Formal analysis, Writing – review & editing. **Lucia Grassi:** Formal analysis, Writing – review & editing. **Gabriele Grassi:** Conceptualization, Writing – review & editing. **Mario Grassi:** Conceptualization, Methodology, Writing – original draft, Writing – review & editing.

Declaration of Competing Interest

The authors declare that they have no known competing financial interests or personal relationships that could have appeared to influence the work reported in this paper.

Data availability

Data will be made available on request.

Acknowledgments

The authors acknowledge Ms. Isabella Peroni for her kind support in the synthesis of hydrogels.

The authors acknowledge Dr. Roberto Melzi (Bruker) for very helpful discussion about the technical aspects of the low-field NMR sequences used.

In addition, the "Programma di valorizzazione dei brevetti del sistema universitario del Friuli Venezia Giulia" - FVG PoC, 2020, Italy, is acknowledged.

Appendix A

It is well known (Melzi, 2020) that the magnetic relaxation time depends on the time separation (τ) between the 90 and 180 pulses of the CPMG sequence. In particular, τ decrease corresponds to the increase of the relaxation time. As this effect becomes more and more important in the case of samples characterized by high relaxation times, its determination requires particular care when dealing with water, the substance characterized by the highest relaxation time in the field of water based systems such as hydrogels.

In order to frame this effect, Fig. A1 reports the water FID decay corresponding to three increasing values of τ. It is qualitatively evident that τ increase implies a faster relaxation process as proved by the lower and lower intercept of the $I(t)$ curve on x axis. The analysis of the three decay curves by means of eq.(8) allows to quantify their differences in terms of the relaxation spectra as depicted in Fig. A2. It is clear that τ increase reflects in the shifting of the whole distribution towards lower relaxation values. In order to quantify this aspect, Fig. A3 reports the displacement of the distribution peak jointly with the displacement of its initial and final point, i.e. the minimum and maximum relaxation time corresponding to $A_{i\%} = 0$. It can be seen that both peak and extremes position increase almost linearly with τ decrease.

Thus, we can say that the real distribution spectrum, i.e. that corresponding to $\tau = 0$, spans from 2546 ms to 3634 ms and shows its peak at 3022 ms. This is the reason why we decided to assume the upper point of the distribution as the free water relaxation time, $T_{2H2O} = 3634$ ms, at 25 °C (20 MHz). Unfortunately, we have to remark that the situation is more complex than we have discussed insofar. Indeed, distribution broadness depends also on the value of the smoothing factor (μ, eq.(12)) adopted to determine the distribution itself. Just as an example, Fig. A4 shows the variation of the water relaxation spectrum assuming five different μ values. We can see that while peak position is not substantially affected by μ variation, distribution broadness increases with μ.

Consequently, while the extrapolation of peak position to $\tau = 0$ holds whatever μ, the distribution wideness should be evaluated for every μ. However, at least in the case of polymeric hydrogels, we found that the optimal μ value according to Wang (Wang and Ni, 2003) spans in between 100 and 300. In this range, the considerations performed for $\mu = 150$ hold as the distribution wideness remains substantially unchanged as suggested by Fig. A4.

Appendix B. Supplementary data

Supplementary data to this article can be found online at https://doi.org/10.1016/j.ijpharm.2023.122882.

References

Abdurrahmanoglu, S., Can, V., Okay, O., 2009. Design of high-toughness polyacrylamide hydrogels by hydrophobic modification. Polymer 50, 5449–5455. https://doi.org/10.1016/j.polymer.2009.09.042.

Abrami, M., Ascenzioni, F., Di Domenico, E.G., Maschio, M., Ventura, A., Confalonieri, M., Di Gioia, S., Conese, M., Dapas, B., Grassi, G., Grassi, M., 2018a. A Novel Approach Based on Low-Field NMR for the Detection of the Pathological Components of Sputum in Cystic Fibrosis Patients. Magn. Reson. Med. 79, 2323–2331. https://doi.org/10.1002/mrm.26876.

Abrami, M., Chiarappa, G., Farra, R., Grassi, G., Marizza, P., Grassi, M., 2018b. Use of low field NMR for the characterization of gels and biological tissues. ADMET DMPK 6, 34–46. https://doi.org/10.5599/admet.6.1.430.

Abrami, M., Marizza, P., Zecchin, F., Bertoncin, P., Marson, D., Lapasin, R., de Riso, F., Posocco, P., Grassi, G., Grassi, M., 2019a. Theoretical Importance of PVP-Alginate Hydrogels Structure on Drug Release Kinetics. Gels. 5 (22), 1–15. https://doi.org/10.3390/gels5020022.

Abrami, M., Siviello, C., Grassi, G., Larobina, D., Grassi, M., 2019b. Investigation on the thermal gelation of chitosan/β-glycerophosphate solutions. Carbohyd. Polym. 214, 110–116. https://doi.org/10.1016/j.carbpol.2019.03.015.

Ahagon, A., Gent, A.N., 1975. Threshold fracture energies for elastomers. J. Polym. Sci. Polym. Phy.s Ed. 13, 1903–1911. https://doi.org/10.1002/pol.1975.180131005.

Akca, O., Yetiskin, B., Okay, O., 2020. Hydrophobically modified nanocomposite hydrogels with self-healing ability. J. Appl. Polym. Sci. 173 (48853), 1–8. https://doi.org/10.1002/app.48853.

Amsden, B. 1998. Solute Diffusion within Hydrogels. Mechanisms and Models. Macromolecules 31, 8382-8395. https://doi.org/ 10.1021/ma980765f.

Amsden, B., 2022. Hydrogel Mesh Size and Its Impact on Predictions of Mathematical Models of the Solute Diffusion Coefficient. Macromolecules 55 (18), 8399–8408. https://doi.org/10.1021/acs.macromol.2c01443.

Bignotti, F., Baldi, F., Grassi, M., Abrami, M., Spagnoli, M., 2021. Hydrophobically-Modified PEG Hydrogels with Controllable Hydrophilic/Hydrophobic Balance. Polymers 13 (1489), 1–15. https://doi.org/10.3390/polym13091489.

Brown, H.R., 2007. A Model of the Fracture of Double Network Gels. Macromolecules 40, 3815–3818. https://doi.org/10.1021/ma062642y.

Brownstein, K., Tarr, C., 1979. Importance of classical diffusion in NMR studies of water in biological cells. Phys. Rev. A 19, 2446–2453. https://doi.org/10.1103/PhysRevA.19.2446.

Ceylan, D., Okay, O., 2007. Macroporous Polyisobutylene Gels: A Novel Tough Organogel with Superfast Responsivity. Macromolecules 40, 8742–8749. https://doi.org/10.1021/ma071605j.

Chui, M., Phillips, R., Mccarthy, M., 1995. Measurement of the porous microstructure of hydrogels by nuclear magnetic resonance. J. Colloid Interface Sci. 174, 336–344. https://doi.org/10.1006/jcis.1995.1399.

Coviello, T., Alhaique, F., Di Meo, C., Matricardi, P., Montanari, E., Zoratto, N., Grassi, M., Abrami, M., 2022. Scleroglucan and Guar Gum: the synergistic effects of a new polysaccharide system. Express Polym Lett 16, 410–426. https://doi.org/10.3144/expresspolymlett.2022.30.

Coviello, T., Matricardi, P., Alhaique, F., Farra, R., Tesei, G., Fiorentino, S., Asaro, F., Milcovich, G., Grassi, M., 2013. Guar gum/borax hydrogel: Rheological, low field NMR and release characterizations. Express Polymer Lett. 7, 733–746. https://doi.org/10.3144/expresspolymlett.2013.71.

Cram, S.L., Brown, H.M., Spinks, G.M., Hourdet, D., Creton, C., 2005. Hydrophobically modified dimethylacrylamide synthesis and rheological behaviour. Macromolecules 38, 2981–2989. https://doi.org/10.1021/ma048504v.

Creton, C., 2017. 50th Anniversary Perspective: Networks and Gels: Soft but Dynamic and Tough. Macromolecules 50, 8297–8316. https://doi.org/10.1021/acs.macromol.7b01698.

De'Nobili, M.D., Rojas, A.M., Abrami, M., Lapasin, R., Grassi, M. 2015. Structure characterization by means of rheological and NMR experiments as a first necessary approach to study the L-(+)-ascorbic acid diffusion from pectin and pectin/alginate films to agar hydrogels that mimic food materials. *Journal of Food Engineering*, *165*, 82-92. https://doi.org/10.1016/j.jfoodeng.2015.05.014.

Draper, N.R., Smith, H. Applied Regression Analysis. 1966. JohnWiley & Sons, Inc., New York, USA.

Fahr, A., Liu, X., 2007. Drug delivery strategies for poorly water-soluble drugs. Expert Opin. Drug Deliv. 4, 403–416. https://doi.org/10.1517/17425247.4.4.403.

Flory, P.J., 1953. Principles of polymer chemistry. Cornell University Press, Ithaca, USA.

Gholap, S.G., Jog, J.P., Badiger, M.V., 2004. Synthesis and characterization of hydrophobically modified poly(vinyl alcohol) hydrogel membrane. Polymer 45, 5863–5873. https://doi.org/10.1016/j.polymer.2004.06.032.

Gong, J.P., Katsuyama, Y., Kurokawa, T., Osada, Y., 2003. Double-Network Hydrogels with Extremely High Mechanical Strength. Adv. Mater. 15, 1155–1158. https://doi.org/10.1002/adma.200304907.

Grassi, M., Grassi, G., Lapasin, R., Colombo, I., 2007. Understanding drug release and absorption mechanisms: a physical and mathematical approach. CRC Press, Boca Raton (FL, USA).

Grinberg, V.Y., Senin, A.A., Grinberg, N.V., Burova, T.V., Dubovik, A.S., Potekhin, S.A., 2018. Energetics of poloxamer micellization at normal and high pressures. Polymer 138, 288–294. https://doi.org/10.1016/j.polymer.2018.01.060.

Gupta, P., Vermani, K., Garg, S., 2002. Hydrogels: From controlled release to pH-responsive drug delivery. Drug Discov. Today 7, 569–579. https://doi.org/10.1016/S1359-6446(02)022559.

Halib, N., Mohd Amin, M.C.I., Ahmad, I., Abrami, M., Fiorentino, S., Farra, R., Grassi, G., Musiani, F., Lapasin, R., Grassi, M., 2014. Topological characterization of a bacterial cellulose - acrylic acid polymeric matrix. Eur. J. Pharm. Sci. 62, 326–333. https://doi.org/10.1016/j.ejps.2014.06.004.

Han, J.O., Lee, H.J., Jeong, B., 2022. Thermosensitive core-rigid micelles of monomethoxy poly(ethylene glycol)-deoxycholic acid. Biomater. Res. 26 (16), 1–11. https://doi.org/10.1186/s40824-022-00263-9.

Haraguchi, K., Takehisa, T., 2002. Nanocomposite Hydrogels: A Unique Organic-Inorganic Network Structure with Extraordinary Mechanical, Optical, and Swelling/De-swelling Properties. Adv. Mater. 14, 1120–1124. https://doi.org/10.1002/1521-4095(20020816)14:16<1120::AID-ADMA1120>3.0.CO,2-9.

Holz, M., Heil, S.R., Sacco, A., 2000. Temperature-dependent self-di†usion coefficients of water and six selected molecular liquids for calibration in accurate 1H NMR PFG measurements. Phys. Chem. Chem. Phys. 2, 4740–4742. https://doi.org/10.1039/b005319h.

Kopač, T., Abrami, M., Grassi, M., Rucigaj, A., Krajnc, M., 2022. Polysaccharide based hydrogels crosslink density equation: a rheological and LF-NMR study of polymer-polymer interaction. Carbohydr Polym. 277 (118895), 1–15. https://doi.org/10.1039/b005319h.

Kopecek, J., 2009. Hydrogels from soft contact lenses and implants to self-assembled nanomaterials. J. Polym. Sci. A Polym Chem. 47, 5929–5946. https://doi.org/10.1002/pola.23607.

Larrañeta, E., Stewart, S., Ervine, M., Al-Kasasbeh, R., Donnelly, R.F., 2018. Hydrogels for hydrophobic drug delivery. Classification, synthesis and applications. J. Funct. Biomater. 9, 13, 1–20. https://doi.org/10.3390/jfb9010013.

Lapasin, R., Pricl, S. Rheology of industrial polysaccharides, Theory and Applications. 1995. Chapman & Hall. London, GB. Pages 374-375.

Latour, L.L., Kleinemberg, R.L., Mitra, P.P., Sotak, C.H., 1995. Pore size distribution and tortuosity in heterogeneous porous media. J. Magn. Resonance A 112, 83–91. https://doi.org/10.1006/jmra.1995.1012.

Latour, L.L., Mitra, P.P., Kleinberg, R.L., Sotak, C.H., 1993. Time-Dependent Diffusion Coefficient of Fluids in Porous Media as a Probe of Surface-to-Volume Ratio. J. Magn. Resonance – Series A 101, 342–346. https://doi.org/10.1006/jmra.1993.1056.

Lee, M.K., 2020. Liposomes for enhanced bioavailability of water-insoluble drugs: In vivo evidence and recent approaches. Pharmaceutics 12 (264), 1–30. https://doi.org/10.3390/pharmaceutics12030264.

Mauri, M., Thomann, Y., Schneider, H., Saalwachter, K., 2008. Spin-diffusion NMR at low field for the study of multiphase solids. Solid State Nucl. Magn. Reson. 34, 125–141. https://doi.org/10.1016/j.ssnmr.2008.07.001.

McKenzie, M., Betts, D., Suh, A., Bui, K., Kim, L., Cho, H., 2015. Hydrogel-Based Drug Delivery Systems for Poorly Water-Soluble Drugs. Molecules 20, 20397–20408. https://doi.org/10.3390/molecules201119705.

Meiboom, S., Gill, D., 1958. Modified spin-echo method for measuring nuclear relaxation times. Rev. Sci. Instrum. 29, 688–691. https://doi.org/10.1063/1.1716296.

Melzi, R. 2020.Time Domain NMR and ProFiler. BRUKER,.

Mezzasalma, S.A., Abrami, M., Grassi, G., Grassi, M., 2022. Rubber elasticity of polymer networks in explicitly non-Gaussian states. Statistical mechanics and LF-NMR inquiry in hydrogel. Int. J. Eng. Sci. 176, 103676, 1–35. https://doi.org/10.1016/j.ijengsci.2022.103676.

Miquelard-Garnier, G., Demoures, S., Creton, C., Hourdet, D., 2006. Synthesis and Rheological Behavior of New Hydrophobically Modified Hydrogels with Tunable Properties. Macromolecules 39 (23), 8128–8139. https://doi.org/10.1021/ma061361n.

Okumura, Y., Ito, K., 2001. The Polyrotaxane Gel: A Topological Gel by Figure-of-Eight Cross-links. Adv. Mater. 13, 485–487. https://doi.org/10.1002/1521-4095(200104)13:7<485::AID-ADMA485>3.0.CO,2-T.

Park, M.H., Park, J., Lee, H.J., Jeong, B., 2020. Alpha-beta transition induced by C18-conjugation of polyalanine and its implication in aqueous solution behavior of poly (ethylene glycol)-polyalanine block copolymers. Biomater. Res. 24 (23), 1–11. https://doi.org/10.1186/s40824-020-00200-8.

Pasut, E., Toffanin, R., Voinovich, D., Pedersini, C., Murano, E., Grassi, M., 2008. Mechanical and diffusive properties of homogeneous alginate gels in form of particles and cylinders. J. Biomed. Mater. Res. A 87A, 808–818. https://doi.org/10.1002/jbm.a.31680.

Pillai, J., Thulasidasan, A.K., Anto, R., Chithralekha, D., Narayanan, A., Kumar, G.S., 2014. Folic acid conjugated cross-linked acrylic polymer (FA-CLAP) hydrogel for site specific delivery of hydrophobic drugs to cancer cells. J. Nanobiotechnol. 12 (25), 1–9. https://doi.org/10.1186/1477-3155-12-25.

Provencher, S.W.A., 1982. A constrained regularization method for inverting data represented by linear algebraic or integral equations. Comput Phys Comm. 27, 213–227. https://doi.org/10.1016/0010-4655(82)90173-4.

Rey-Rico, A., Cucchiarini, M., 2018. PEO-PPO-PEO tri-block copolymers for gene delivery applications in human regenerative medicine - an overview. Int. J. Mol. Sci 19 (775), 1–15. https://doi.org/10.3390/ijms19030775.

Saalwachter, K., Chassea, W., Sommer, J.U., 2013. Structure and swelling of polymer networks: insights from NMR. Soft Matter 9, 6587–6593. https://doi.org/10.1039/c3sm50194a.

Saalwachter, K., 2003. Detection of Heterogeneities in Dry and Swollen Polymer Networks by Proton Low-Field NMR Spectroscopy. J. Am. Chem. Soc. 125, 14684–14685. https://doi.org/10.1021/ja038278p.

Scherer, G.W., 1994. Hydraulic radius and mesh size of gels. J. Sol Gel Sci. Technol. 1, 285–291. https://doi.org/10.1007/BF00486171.

Schurz, J., 1991. Rheology of polymer solutions of the network type. Prog. Polym. Sci. 16, 1–53. https://doi.org/10.1016/0079-6700(91)90006-7.

Singh, N.K., Lee, D.S., 2014. In situ gelling pH- and temperature-sensitive biodegradable block copolymer hydrogels for drug delivery. J. Control Release 193, 214–227. https://doi.org/10.1016/j.jconrel.2014.04.056.

Skirda, V.D., Aslanyan, I.Y., Philippova, O.E., Karybiants, N.S., Khokhlov, A.R., 1999. Investigation of translational motion of poly(ethylene glycol) macromolecules in poly(methacrylic acid) hydrogels. Macromol. Chem. Phys. 200, 2152–2159. https://doi.org/10.1002/(SICI)1521-3935(19990901)200:9<2152::AID-MACP2152>3.0.CO,2-M.

Staltari, G., Biasin, A., Grassi, L., Gerin, F., Maschio, M., Confalonieri, M., Grassi, G., Grassi, M., Abrami, M., 2022. Rheological and Low Field NMR Characterisation of Cystic Fibrosis Patient's Sputum. Chem. Biochem. Eng. Q. 36, 239–253. https://doi.org/10.15255/CABEQ.2022.2119.

Tanaka, Y., Gong, J.P., Osada, Y., 2005. Novel hydrogels with excellent mechanical performance. Prog Polym Sci 30, 1–9. https://doi.org/10.1016/j.progpolymsci.2004.11.003.

Tencho, B.G., Yanev, T.K., 1986. Weibull distribution of particle sizes obtained by uniform random fragmentation. J. of Coll. and Int. Sci. 111, 1–7. https://doi.org/10.1016/0021-9797(86)90002-0.

Turco, G., Donati, I., Grassi, M., Marchioli, G., Lapasin, L., Paoletti, S., 2011. Mechanical Spectroscopy and relaxometry on alginate hydrogels: a comparative analysis for structural characterization and network mesh size determination. Biomacromolecules 12, 1272–1282. https://doi.org/10.1021/bm101556m.

Vhora, I., Lalani, R., Bhatt, P., Patil, S., Patel, H., Patel, V., Misra, A., 2018. Colloidally stable small unilamellar stearyl amine lipoplexes for effective BMP-9 gene delivery to stem cells for osteogenic differentiation. AAPS PharmSciTech 19, 3550–3560. https://doi.org/10.1208/s12249-018-1161-6.

Volpert, E., Selb, J., Candau, F., 1998. Associating behaviour of polyacrylamides hydrophobically modified with dihexylacrylamide. Polymer 39, 1025–1033. https://doi.org/10.1016/S0032-3861(97)00393-5.

Volpert, E., Selb, J., Candau, F., 1996. Influence of the Hydrophobe Structure on Composition, Microstructure, and Rheology in Associating Polyacrylamides Prepared by Micellar Copolymerization. Macromolecules 29, 1452–1463. https://doi.org/10.1021/ma951178m.

Wang, X., Ni, Q., 2003. Determination of cortical bone porosity and pore size distribution using a low field pulsed NMR approach. J Orthop Res. 21, 312–319. https://doi.org/10.1016/S0736-0266(02)00157-2.

Whittal, K.P., MacKay, A.L., 1989. Quantitative interpretation of NMR relaxation data. J Magn Reson. 84, 134–152. https://doi.org/10.1016/0022-2364(89)90011-5.

Wichterle, O., Lím, D., 1960. Hydrophilic Gels for Biological Use. Nature 185, 117–118. https://doi.org/10.1038/185117a0.